Impact of multi-scale dynamical processes and mixing on the chemical composition of the upper troposphere and lower stratosphere during INTEX-NA

T. Duncan Fairlie[1], Melody A. Avery[1], R. Bradley Pierce[1], Jassim Al-Saadi[1], Jack Dibb[2], Ron Cohen[3], Glen Sachse[1]

[1]NASA Langley Research Center, Hampton, VA-23681
[2]University of New Hampshire, Durham, NH.
[3]University of California, Berkeley, CA.

August 14, 2006

Abstract:

We use high frequency in situ observations made from the DC8 to examine fine-scale tracer structure and correlations observed in the upper troposphere and lower stratosphere during INTEX-NA. Two flights of the NASA DC-8 are compared and contrasted. Chemical data from the DC-8 flight on July 18 shows evidence for interleaving and mixing of polluted and stratospheric air masses in the vicinity of the subtropical jet in the upper troposphere, while on August 2 the DC-8 flew through a polluted upper troposphere and lower stratosphere (middle world) that were more distinctly separated. We compare data from both flights with RAQMS 3-d global meteorological and chemical model fields to establish dynamical context, and to diagnose processes regulating the degree of mixing on each day. We also use trajectory mapping of the model fields to show that filamentary structure due to upstream strain deformation contributes to tracer variability observed in the upper troposphere. Higher frequency (6 – 24 km) tracer variability is attributed to buoyancy wave oscillations in the vicinity of the jet, whose turbulent dissipation leads to efficient mixing across tracer gradients. A measure of strain and rotation in the large-scale flow, Q, is found useful in predicting filamentary structure in the vicinity of the jet for the cases considered but limited in predicting the higher frequency gravity wave modes.

1. **Introduction**

During the summer of 2004 the NASA DC-8, carrying a comprehensive chemical sensor payload, participated in a major aircraft field campaign making measurements over North America in the troposphere and lowermost stratosphere. The Intercontinental Chemical Transport Experiment – North America (INTEX-NA) was designed to understand the transport and transformation of gases and aerosols on transcontinental/ intercontinental scales, and their impact on air quality and climate [Singh et al., this issue]. Particular

goals of INTEX-NA were to characterize fluxes of ozone and its precursors to and from the North American continent, and to provide correlative measurements to validate observations from satellites. The INTEX-NA measurements were a critical part of a much larger, multi-agency effort, ICARTT, described by Fehsenfeld et. al., 2006. Together, measurements and modeling efforts associated with INTEX-NA and ICARTT provide a rich data set from airborne and ground-based remote sensors, sonde and aircraft-based in-situ instrumentation, and modeled chemical fields, spanning a wide range of temporal resolution and spatial scales.

A fundamental issue in Earth science is to quantify the human impact on the climate and composition of the earth's atmosphere. Much effort has been focused on quantifying the impact of anthropogenic emissions of photochemically active gases and aerosols on air quality, the oxidizing capacity of the atmosphere (Logan et al., 1981; Chameides and Davies, 1982) and climate (Fishman et al., 1979; Jacob and Gilliland, 2005, and references therein). There has also been much effort to distinguish the impact of ozone produced via pollution in the troposphere from that originating in the stratosphere (e.g. Fishman and Crutzen, 1977; Liu et al., 1980; Shapiro, 1980; Wang et al., 1998; Logan, 1985). Much of the difficulty in pursuing this latter objective is that transport processes, responsible for redistributing ozone and its precursors in the atmosphere, operate on a wide range of spatial and temporal scales, from planetary scale motions that move material quasi-isentropically to small-scale intermittent processes like convection and turbulence that can redistribute material across isentropes. This presents a serious challenge for global and regional scale models that are used to make such quantitative assessments. The models can capture transport processes at grid and higher scales, but sub-grid-scale processes must be parameterized. Because laminae of both stratospheric and polluted air are commonly observed in the upper troposphere, differentiation of anthropogenic effects from natural variability is difficult.

The upper troposphere and lower stratosphere are critical regions for assessing the human impact on radiatively active trace gases such as ozone,

because radiative forcing due to changes in such gases is most sensitive in this region (Forster and Shine, 1997). Of particular interest is the region around upper tropospheric jet streams. These jets are characterized typically by strong horizontal and vertical wind shears, thermal gradients, and associated cross-jet gradients in potential vorticity and chemical constituents, which provide a natural separation between the troposphere and stratosphere. Transport along a jet can be very rapid so that anthropogenic pollution lofted from below can have a significant long-range (intercontinental) component and diverse origins. Convective and pre-frontal (warm conveyor belt) lifting during cyclogenesis can bring boundary layer pollutants into close proximity with stratospherically influenced air subsiding in dry tongues behind upper frontal systems (Cooper et al., 2004; Elser et al., 2003). Strong accelerations in the vicinity of jet streaks and strong curvature lead to tropopause folding and isentropic exchange of air through tropopause breaks (Danielsen et al., 1991; Shapiro, 1980). Jets also support a wide range of spatial and temporal scales of motion, from inertial (Rossby) waves that propagate upon lateral gradients in potential vorticity to buoyancy waves, and turbulence driven by vertical shear. Planetary wave breaking in regions of strong cross-tropopause tracer gradients can lead to filamentation and intermediate-scale horizontal variability in quasi-conserved chemical species like ozone (Appenzeller et al., 1996) via stretching of tracer gradients along streamlines. Smaller-scale inertio-gravity or high frequency gravity waves can perturb the alignment of isentropic surfaces where tracer gradients are large (Danielsen et al., 1991; Chan et al., 1991) and can lead to irreversible mixing of chemical characteristics across air mass interfaces (Shapiro, 1980; Cho et al., 1999).

Thus, the generation of small-scale tracer structure in the vicinity of upper tropospheric jets and boundaries between polluted and stratospheric air masses can have important consequences for exchange of air across the tropopause and the irreversible mixing of polluted and stratospheric air masses. Understanding and quantifying irreversible material exchange across the tropopause, and mixing of air of differing origins in that region is a goal of the broader scientific

community, including that of INTEX-NA. The goal in this paper is to provide improved characterization of the impact of dynamical and transport processes on the chemical composition of the upper troposphere and lowermost stratosphere during INTEX-NA, and to differentiate the effects of planetary-scale motions from smaller-scale buoyancy and turbulent motions. We use high frequency aircraft in situ chemical observations made from the DC8 to characterize fine-scale tracer structure, and use constituent correlations to distinguish air of different origins. We use a global 3-d model, RAQMS (Pierce et al., 2004), to provide dynamical context and insight into larger-scale transport processes to aid interpretation of the observational data. We apply a trajectory mapping technique (reverse domain filling, or RDF) to the global model fields to assess the extent to which upstream strain deformation contributes to small-scale variability observed in the tracer fields, and use a measure of large-scale strain and rotation, Q, (Haynes, 1990) to identify regions where filamentation is expected to occur. RDF has been used to explain the development of small-scale tracer structure in the stratosphere (Fairlie et al., 1997). Questions posed here include: Can RDF be used to explain some of the small-scale tracer variability observed from the DC8? Can the Q field provide useful information on the preferred locations where small-scale tracer structure is found?

To answer these questions we compare and contrast two flights of the DC-8 during the INTEX-NA deployment to Pease, New Hampshire. The two flights occurred over a similar geographical region of New England, Eastern Canada and the western Atlantic. The DC-8 sampled the upper troposphere in the vicinity of the subtropical jet on both flights. Measurements suggest that the upper troposphere was significantly polluted, as well as stratospherically influenced. However, the two flights were found to have a contrasting degree of tracer variability, differing pollution sources, and varying amounts of mixing between stratospheric and tropospheric air. We use the RAQMS model to examine differences in the meteorological context and chemical transport environment of the flights, and in situ chemical and dynamical variables to interpret the observed structure and processes at work.

2. Tools/Methods

2. In Situ Measurements and Merged Data

The NASA DC-8 contained a full payload of instruments making photochemical measurements during INTEX-NA. In this paper we focus on the in situ measurements of ozone, carbon monoxide, nitric acid and total peroxynitrates (TPNs). The in situ ozone and carbon monoxide measurements were made at 1 second temporal resolution by nitric oxide chemiluminesence (Avery et. al., 2006) and by diode laser spectrometer (Sachse et al.). TPNs were measured by thermal dissociation and laser induced fluorescence, with a data collection cycle of 25 seconds (Thornton et al., 1999), and include both PAN and pernitric acid, HNO4. Nitric acid was measured by mist chamber collection at 100 seconds (Dibb et al., this issue) Two merged chemical data sets were created, one at 1 second to correlate the fast data streams, and the other at 100 seconds, corresponding to nitric acid sampling times. All reported TPN data was averaged over the longer nitric acid measurement cycle for inclusion in the slower merged data stream.

2.2. RAQMS Model Description

The 3-d model used in this study is the LaRC/UW Realtime Air Quality Modeling System (RAQMS) (Pierce et al., this issue). RAQMS is a portable, global- to regional-scale meteorological and chemical modeling system which has been developed for assimilating remote observations of atmospheric chemical composition and predicting air quality globally or regionally (Pierce et al., 2004). RAQMS ozone fields are constrained via assimilation of satellite ozone column and profile measurements. This study uses a global simulation

conducted for the INTEX-NA period. Pierce et al. (this issue) present an evaluation of the RAQMS simulation and an analysis of the continental US O3 and NOy budgets. Al-Saadi et al. (this issue) use trajectory mapping to identify the dominant contributions to O3 distributions over the INTEX domain and Europe, and their air mass origins. The global component of RAQMS has at its dynamical core the University if Wisconsin (UW) global hybrid model (Zapotocny et al., 1991, Zapotocny et al., 1994). The RAQMS unified stratosphere/troposphere chemistry module has been developed to represent photochemical processes governing ozone formation and destruction within Earth's atmosphere from the surface to about 60 km. Full details the chemical formulation are given by Pierce et al. (this issue)

2.3 Langley Trajectory Model (LTM)

3-d trajectory calculations are conducted using a new version of the Langley trajectory model (LTM) (Pierce and Fairlie, 1993; Pierce et al., 1994) that has been configured to use RAQMS hybrid coordinate wind fields. The LTM has been used to explore the kinematics of mixing, tracer filamentation and variability due to large scale flow fields in the stratosphere (Pierce et al., 1994; Fairlie et al., 1997), and has been used to characterize sources and chemical transformations during INTEX-A (Al-Saadi et al., this issue). It is currently used as the trajectory component of the Infusing Satellite Data into Environmental Applications (IDEA) program to provide real-time PM2.5 air quality forecast guidance (Al-Saadi et al., 2005).

In this study, the LTM is used to construct reverse-domain-filled (RDF) ozone fields along aircraft flight tracks to compare with the measured in situ ozone data. The LTM samples global chemical and dynamical fields from the RAQMS model. RDF is a trajectory mapping technique that has shown potential to represent coarsely resolved constituent fields at higher resolution, with higher information content, than originally observed (Sutton et al., 1994) (or modeled). Here, we use RDF to assess how much tracer variability observed along aircraft flight tracks during INTEX can be explained by large-scale dynamical processes

(such as Rossby wave-breaking) and intermittent diabatic processes captured within the RAQMS modeling system. Fairlie et al. (1997) cautioned that RDF generally does not show skill in adding small-scale information when applied to fields of highly derived quantities, e.g. PV, but can provide useful information when it refines structure that already exists in conventional analyses. Its application to dynamically and chemically consistent ozone analyses from RAQMS is expected to be more fruitful. RDF is not expected to add quantitative information on tracer variability due to small-scale dynamical processes that are not explicitly represented in RAQMS, e.g. gravity waves, turbulence.

2.4 Mixing diagnostic

We use a measure of the relative contribution of strain and rotation in the large-scale flow, Q, to explore whether such a diagnostic can be used as an objective synoptic-scale predictor of intermediate to small-scale ozone variability in the upper troposphere. Haynes (1990) found that positive Q is associated with regions of Rossby wave breaking where efficient stirring of air masses occurs, while negative Q is associated with closed circulations. Efficient stirring promotes irreversible mixing by increasing interfacial area between distinct air masses. Q has been used as a measure the mixing efficiency of trace gases on isentropic surfaces in regions of strong gradients and planetary wave breaking (Fairlie et al., 1999; Pierce et al., 2003). Here, we compute time-averaged Q following air parcel back trajectories and explore whether this quantity can provide information on small-scale tracer variability observed in the upper troposphere during INTEX-A.

3. Comparison of Upper Tropospheric In Situ Observations on 18 July and 02 August

In this section, we compare and contrast chemical tracer variability and correlations observed on 2 flights during INTEX-A, those of 18 July and 02 August. The two flights were selected because they took place over a similar geographical region of New England, Eastern Canada, and the Atlantic

seaboard, yet the DC-8 measurements indicate significant differences in composition and structure in the upper troposphere on these days.

Figure 1 shows GOES 12 IR water vapor images for 1745Z for those flight days. The flight tracks are superimposed and the vertical flight profiles are inset (images courtesy of D. Westberg, SAIC). On July 18, there was a deep trough over the eastern U.S., with a developing low pressure system centered over the Carolinas. Widespread clouds associated with the low are visible in the satellite image. The upper troposphere along the flight track was affected by a split flow, with a confluent region between the polar and subtropical jets encountered near points 3 and 6. On August 2, a subtropical high dominated much of the area, with mostly clear skies and subsiding air. Unlike 18 July the subtropical jet did not extend deep into the southeast United States but was more zonally orientated near the Canadian border. As a result, except for the most northern part of the flight, the DC-8 remained on the equator side of the jet, whereas on July 18 the flight track took place primarily on the poleward side of the jet. The DC8 flight track included several level flight legs (FLs) in the upper troposphere on each day. We have numbered the locations of these legs in sequence on each panel for reference.

Figure 2 shows time series of in situ ozone measured during each flight (left). The ozone time series (black) are shown together with the altitude of the aircraft (orange). On 18 July the ozone data shows considerable small-scale, high-amplitude variability for several of the upper-level, constant-pressure flight legs (FLs). Spectral analysis (not shown) reveals that average and peak amplitudes of oscillations on timescales in the range 30s to 10min on upper-level flight legs are typically 2 to 3 times those found on corresponding upper-level flight legs on 02 August. (For example, the average amplitude at 100s is 5 ppb on 18 July, but only 1 ppb on 02 August). This study aims to illuminate the reasons for the different intensities of small-scale O3 variability encountered on these 2 flights and the processes responsible for the small-scale structure encountered on 18 July.

Correlations between ozone and other trace gases also appear considerably different on these two days. The middle and right hand panels of Fig.2 show scatter plots of CO vs. O3 (middle) and HNO3 vs. O3 (right) for observations made above 500 mb on both days. We examine CO and HNO3 because CO is a tropospheric combustion tracer that is anticorrelated with stratospheric ozone, while HNO3 has a significant stratospheric source that is positively correlated with stratospheric ozone. Observations on FLs 3 (stratospheric influence) on each day are highlighted in orange. To put these flights in a larger context, 2-d probability distributions (pdfs) of all observations made above 500 mb from the DC-8 between July 6 and August 7 (except for the 2 flight days of our focus) are contoured on the correlation plots. The pdfs show the densest clustering of upper tropospheric observations during INTEX-A occurred at O3 mixing ratios of ~ 80 ppb, CO ~ 100 ppb and HNO3 < 300 ppt, which might be considered an upper tropospheric "background" measured during INTEX-NA. Each correlation plot shows tropospheric and stratospheric branches. Tropospheric pollution is characterized by enhanced CO and HNO3 for O3 ~ 80 -100 ppb, with higher O3 for photochemically altered air. Extremely high CO, (up to 600 ppbv of CO was measured), and high HNO3 observed on 18 July, with no O3 enhancement, were associated with smoke from Alaskan fires. Many of the other observations with relatively high CO and HNO3 and elevated ozone on 18 July were associated with convective outflow. On 02 August, the majority of the measurements show higher O3 values on the tropospheric branch of both scatter plots. Hydrocarbon and reactive nitrogen ratios (not shown) measured in the upper troposphere during this flight are characteristic of aged pollution.

The stratospheric branch of the correlation plots is characterized by a positive correlation between HNO3 and O3, with a slope of approximately 3.5 ppt:1 ppb (Dibb et al., this issue), and a negative correlation of CO and O3. On each of the 2 flight days, many of the points on this latter branch are from FL 3 (orange). On 18 July, FL 3 is characterized by a mixing line connecting the stratospheric and tropospheric branches on both CO and HNO3 correlation plots.

These observations provide evidence of mixing of stratospheric and polluted air masses in the upper troposphere on this day. On 02 August the DC8 clearly sampled the lower stratosphere (middle world) on FL3 with O3 values in excess of 300 ppb and CO ~ 50 ppb. Measurements of enhanced beryllium-7 (not shown) confirm that the DC8 was flying in the stratosphere.

Next we examine HNO3, ozone and PAN together to compare observational with modeled differentiation between tropospheric and stratospheric air. Since PAN formation requires hydrocarbon oxidation products, it has a source in the polluted troposphere, but has a lifetime of months to years in the cold upper troposphere and middle world. In comparison, nitric acid is soluble, has a stratospheric source and is positively correlated with ozone in stratospheric air (Dibb et. al., 2006). We use measured TPN, rather than PAN because it is available at higher frequency than PAN measurements. The TPN measurement includes pernitric acid (HNO4); HNO4 measurements (Kim et. al., this issue) on the stratospheric flight legs (FLs 3) on both days ranged between 58-79 pptv.

Figures 3a and 3b show flight curtains of ozone, HNO3 and TPN (PAN+HNO4) from the RAQMS model for the 2 flight days with the DC8 altitude profiles superimposed. Isotachs (white) and isentropes (black dashed) are also shown. Time series of the in situ observations are shown in the lower panels (black), with time series of RAQMS data interpolated to the flight altitude superimposed (red). As shown on the flight curtain on 18 July, the DC-8 approaches the subtropical jet, shown by peak wind speeds > 40 ms^{-1} and diverging isentropic surfaces, near 1750Z from the west (poleward side) before turning to the north. Later, the DC-8 crossed the jet from north to south near 2020Z. FLs 2, 3, and 6, which showed most high-frequency variability (Fig.1), occurred on the poleward side of the jet, just beneath where RAQMS indicates large vertical ozone and HNO3 gradients marking the transition between troposphere and lower stratosphere. RAQMS shows a polluted southwesterly air stream (characterized by elevated PAN) in the mid to upper troposphere. High values of HNO3 in the boundary layer and free troposphere are characteristic of

fresh pollution. Extremely high HNO3 and TPN in the RAQMS fields near 1900Z result from simulated emissions from Alaskan fires. The DC8 sampled TPN > 500 ppt during profiling to FLs 2, 3, 6 and 7. These values were not fully captured by RAQMS, reflecting a low bias for simulated PAN in the upper troposphere and lower stratosphere (Pierce et al., this issue). RAQMS is typically 20% high compared with observed O3 in the upper troposphere (Pierce et. al. this issue), and also shows a high bias for HNO3 in the upper troposphere. Compared with the 1-sec. in situ data, the RAQMS analyses show limited variability on each upper-level flight leg. RAQMS analyses have a resolution of 1.4 deg. by 1.4 deg and thus can represent structure only on scales greater than about 150 km (~12 minutes flight time). TPN observations indicate that small-scale ozone variability on upper level FLs 2 and 3 is also characteristic of longer-lived tropospheric pollutants.

The flight curtain on 02 August crosses the jet from south to north near 1500Z (~ 48^{o}N) and re-crosses the jet near 1930Z. The curtains show FL3 clearly penetrating vertical ozone and HNO3 gradients, associated with the depressed tropopause on the poleward side of the jet, into the middle world, where O3 > 300 ppb and HNO3 > 1000 ppt were observed. Very dry air with H2O around 20 ppm, and beryllium-7 values around 7000 ppt were also observed (not shown). Of particular note, TPN in excess of 300 ppt was observed on FL3, with HNO4 concentrations of 78 ppt or below, indicating tropospheric pollution has reached the lower stratosphere. These observations are consistent with the deduction by Pierce et al. (this issue) of isentropic troposphere to stratosphere fluxes at the subtropical tropopause break in the INTEX domain. FLs 2, 6 and 7, which took place equatorward of the jet core indicated a polluted air stream in the middle to upper troposphere, characterized by TPN > 500 ppt, high organics, low NOx/NOy, and elevated O3. RAQMS shows good agreement with observed O3 along the flight track, except for the stratospheric flight leg (FL 3) where both O3 and HNO3 are underpredicted.

Figure 4 shows maps of PV and O3 at 18Z for 18 July (330K) and 02 August (335K) from the RAQMS model. The DC8 flight tracks are superimposed,

together with the location of selected high-altitude flights legs. Also shown are isotachs (contoured), wind vectors, and the axis of strongest winds (white line). The deep trough over the eastern U.S. on 18 July is distinguished by higher O3 and PV. The PV and O3 structure is reminiscent of “Type II” (cyclonic rollup) Rossby wave breaking (Appenzeller et al., 1996). In contrast, on 02 August the 335K maps show a more zonal jet with evidence of weaker “Type I” (anticyclonic) wave breaking south of the jet with remnants of high PV and ozone drawn into the short-wave trough over the eastern U.S. and a streamer of high ozone (~120ppb) extending southward on the east of the flight track, near 60W. Both flight tracks span the axis of strongest winds but most of the track on 18 July (in particular FLs 2,3, and 6) lay north of the jet core, whereas on 02 August the flight track lay primarily south of the jet. FL3 on 18 July occurs in a region of jet confluence where isentropic descent of air parcels and tropopause folding is expected.

Cross-sections of PV, O3, HNO3 and TPN taken along the lines A-B and C-D in Fig.4 are shown in Fig. 5. The cross-sections provide a cross-jet perspective of the tracer structure in RAQMS and emphasize the change in tropopause elevation across the jet. Projection of the flight altitude and latitude on to the cross-sections emphasizes the relative positions of the upper level flight legs on each day with respect to the jet. Cross-sections for July 18 show further evidence that FLs 2, 3 and 6, which showed enhanced small-scale ozone variability, occurred poleward of the jet core at 45^{o}N, just below a depressed tropopause. FL 7, which showed much less variability, occurred farther south on the equatorside of the jet. The cross-sections for 02 August show the ascent of the DC8 into the middle world (FL3) on the poleward side of the jet at 48^{o}N to FL3. Only FLs 3 and 4 occurred poleward of the jet on this day.

The scatter plots in Fig.2 clearly indicate that the DC8 sampled a mixture of tropospheric and stratospheric air poleward of the jet core on 18 July. In situ observations of TPN (Fig.3) indicate significant concentrations of PAN in the middle world on 02 August. Given the long lifetime of PAN in the UT/LS this indicates that an incursion of polluted air into the lowermost stratosphere. Figure

6 shows scatter plots of observed and simulated HNO3 vs. O3 for points above 500 mb, colored by the TPN mixing ratio. The observational data are shown at the frequency of the HNO3 measurements. Highest PAN values are associated with the Alaskan fires (18 July) and with the aged tropospheric pollution (02 August). The marked range of TPN values on the stratospheric branches of the scatter plots [from under 100 to above 400 ppt] are a further indication of sporadic exchange and mixing between polluted tropospheric and stratospheric air. These observations caution us that the collocation of high O3 with high PAN does not necessarily indicate that the high O3 was photochemically produced. RAQMS generally represents the pollution and stratospheric branches in HNO3 vs. O3 on 18 July, but does not capture the full range of TPN values on each. On 02 August RAQMS shows the stratospheric branch in HNO3 vs. O3 space, but underestimates the high TPN and HNO3 associated with the tropospheric pollution branch. In addition, RAQMS underestimates highest values of O3 and HNO3 associated with the incursion into the middle world, and the range of TPN values observed there. Underestimates in convective or lightning NOx sources could account for the underestimation of upper tropospheric TPN in the model. Limited vertical and horizontal model resolution near the tropopause likely explains the model's inability to fully capture the tracer variability, and indicates that the associated dynamics and mixing processes operate at the subgrid-scale.

4. The impact of large-scale deformation: filamentation due to Rossby wave breaking

In comparing the flights of July 18 and August 02, we stressed that the flight legs that show highest levels of small-scale ozone variability occurred beneath a depressed tropopause on the poleward side of the jet. One mechanism that could contribute to the observed ozone variability on these flight legs is the vertical deformation (folding) of the tropopause and differential advection (shear strain) in regions of jet acceleration and upper-level cyclogenesis as a result of Rossby wave amplification. Rossby wave amplification can locally enhance PV, temperature and constituent gradients at

the tropopause, can lead to the development of cutoff lows and highs, and at smaller scales the interweaving of tropospheric and stratospheric air in long streamers or filaments (Appenzeller et al., 1996; Holton et al., 1995).

To explore the contribution of large-scale deformation to the tracer variability observed from the DC8 on the upper level flight legs, we conducted back trajectory simulations and applied a reverse-domain-filling (RDF) trajectory mapping technique to RAQMS analyses of the DC8 flight curtain (Fig.2), and to selected horizontal surfaces. Back trajectories were conducted using the LaRC trajectory model (Al-Saadi et al., this issue). Chemical and dynamical fields from RAQMS were sampled along the trajectory paths, and Lagrangian averages of these fields were mapped to the initial parcel locations. The RDF method is intended to provide information about tracer variability which can be attributed to large-scale deformation, but at scales smaller than those that can be represented in conventional analyses. The premise of RDF is that it simulates the physical cascade of tracer variability to small scales due to large-scale deformation (Sutton et al., 1994). A similar premise applies to the contour advection technique (Norton, 1994; Waugh and Plumb, 1994). For the flight curtain, air parcels were initialized at 1-minute intervals on RAQMS vertical grid from the ground to the lower stratosphere; for mapped RDF products, parcels were initialized on a uniform grid of 0.5 deg. by 0.5 deg. The RDF products shown here are 2-day Lagrangian averages of selected quantities sampled at 2-hour intervals along air parcel back trajectories.

Figure 7 shows 2-day RDF O3 along the flight curtain for 18Z on July 18 with the DC8 flight profile superimposed. A time-series of the in situ ozone is also shown, together with the analyzed and RDF time series from RAQMS. The top two panels may be compared with those shown in Fig.2. The lower two panels in Fig.7 are local expansions of the time series plot for time periods encompassing FLs 3 and 7 respectively. The RDF time series adds some information about the time evolution of ozone on FL3, notably a single wave-like oscillation along the flight leg, that is discernable in the data but not so in the RAQMS analysis. In addition, the RDF series is better correlated (r = 0.76) than the analyzed series (r

= 0.59) with 1-min averaged in situ ozone data for FL3. On the other hand RDF shows a higher bias for FL3 verses observations. For FL7, which shows little observed variability RDF introduces no significant additional structure. The 2-day RDF provides no information about ozone variability at scales smaller than about 10 minutes, suggesting that processes other than large-scale deformation are responsible.

Figure 8 shows maps of 2-day RDF ozone, Lagrangian pressure change (Δp) and RDF Q at 330K for 18Z on 18 July. The Lagrangian Δp map shows the vertical displacement of parcels in the previous 2 days ($\Delta p > 0$ (< 0) corresponds to descent (ascent)). The RDF O3 map may be compared with the corresponding analysis shown in Fig.4. The map shows a narrow filament of high ozone crossing the flight track just east of FL3 on the western flank of the jet, composed of parcels that have descended strongly in the previous 2 days. The elongated structure is consistent with upstream descent and cross-jet differential advection, characteristic of upper level frontal development. Parallel to the ozone streamer on the eastern side of the jet are parcels ascending in a warm conveyor belt, associated with the cyclonic development ($\Delta p < -100$ mb day^{-1}). The RDF map also shows a number of refinements of features in the ozone analysis in Fig.4. Notably, the streamer of elevated ozone stretched across the DC8 flight track near FL3 is shown to be a refinement of a high ozone anomaly in Fig.4. This streamer appears as an O3 maximum in latter half of FL3 (Fig.7)and shows up on the flight curtain as a narrow fold of high ozone extending downward on the poleward side of the jet. We see now that the high O3 bias introduced by RDF for FL3 (Fig.7) is due to descent. In addition, the RDF map indicates the high ozone air mass enclosed in the deep upper level trough joined to stratospheric air on the polar side of the polar jet near 60 N, which the DC8 sampled near FL6 at 1915Z. The ozone structure within the upper trough fits the pattern of a Type II (cyclonic) intrusion and rollup of stratospheric influenced air into the upper troposphere (Appenzeller et al., 1996). The western flank of the upper level trough (eastern flank of the upstream ridge) is a preferred region for adiabatic

descent and folding of the tropopause and for Rossby wave breaking (Holton et al., 1995; Appenzeller et al., 1996; Postel and Hitchman, 1999).

We use RDF Q to distinguish air masses that have experienced significant horizontal shear strain deformation over the previous 2 days from those that have stayed under more coherent, rotational conditions. The RDF map of Q for 18 July in Fig.8 shows negative values characteristic of rotational flow for air parcels within the upper trough and in the high-pressure system southeast of the flight track. Large, positive values characteristic of shear strain deformation are found on the outer flanks of the trough, the upstream ridge, and the offshore anticyclone and in regions of strong shear associated with the polar and subtropical jets. Notice that the streamers of high O3 in the vicinity of the flight track are closely aligned with high values of Q, consistent with a shear-driven origin for these streamers. Although RDF Q is also positive near FL7, this has little impact on ozone variability since FL7 is not close to strong ozone gradients. In addition, RAQMS indicates that air parcels in the vicinity of FL7 experienced convection in the upper trough in the previous 48 hours, which would tend to homogenize the air parcel chemical characteristics, and could account for the relative uniformity of observed ozone on that flight leg.

Figure 9 shows RDF ozone for the flight curtain on 02 August, together with observed and simulated ozone time series, and expanded time series focused on FLs 3 and 6 for that day. RDF adds some information about the ozone variability present in the RAQMS analyses for these FLs (the correlation with 1-min averaged in situ ozone data increases from 0.68 for the analyzed to 0.75 for the RDF ozone time series for FL3), but the RDF ozone is higher on FL3 compared with the analysis, improving the comparison with observations. The RDF map of ozone (not shown) indicates strong localized descent and downwelling of higher ozone on the poleward flank of the jet in the region sampled by FL3, but RDF makes only minor refinements and little additional refinement of features on the analyzed map of O3 (Fig.4). FL3 on 02 August shows moderate levels of variability with a peak to trough range of up to 60 ppb despite the DC8 sampling a relatively small area on this FL due a circuital track

(Fig. 1). Like those FLs on July 18 that showed enhanced variability FL3 on August 02 occurred on the poleward side of the jet.

5. The origin of smaller-scale variability

The above examination indicates that filamentation associated with descent and differential advection on the poleward side of the jet can explain some of the larger-scale features encountered on level flight legs on 18 July. However, the in situ data shown in Fig.7 indicates significant energy at finer scales in the o3 time series. Danielsen et al. (1991) and Chan et al. (1991) examined tracer and dynamical structure in the vicinity of the subtropical jet during the 1984 STEP campaign. Chan et al. found evidence for a vertically propagating elliptically polarized inertio-gravity wave in the low stratosphere, while Danielsen et al. illustrated the perturbation of tracer gradients by such a wave, and diagnosed the existence of higher-frequency buoyancy waves that can lead to irreversible mixing across tracer gradients. Here we examine how ozone variability observed on 18 July is related to temperature and wind perturbations and assess the extent to which wave motions can to account for the observed small-scale ozone structures.

To conduct this analysis we took the 1-sec. time series of O3, theta, u and v velocity components on FL3 and constructed 10-sec. average data, in order to account for the lower sampling frequency for temperature measurements on the DC8. We removed linear trends from the 10-sec. data and applied a “medium pass filter,” eliminating oscillations with periods less than 250 seconds (~ 50km of level flight). This limit was suggested by a local minimum in the power spectrum for O3 along FL3. Normalized (high frequency) residuals of O3 and theta were obtained as differences between the filtered data and the 10-sec. data divided by the filtered data. We followed a procedure analogous to that of Pierce and Grant (1998) in scaling the theta residuals by the ratio of the normalized derivatives of filtered O3 to filtered theta along FL3 to account for differences in the medium-scale gradients of O3 and theta.

Figure 10 shows the results of this procedure for O3 and theta. We recall that on FL3 the DC8 approaches the jet core from the west. Panels (a) and (b) show 10-sec. O3 and theta respectively on FL3, together with linear trends (dashed), and filtered data (dotted). The normalized residuals of O3 and theta are shown in panel (c), together with a running profile of the cross-correlation coefficient, evaluated in 5-minute intervals. The residuals show significant energy for time scales in the range 30 sec. to 120 sec. (~ 6 to 24 km). The O3 and theta residuals are highly correlated in the middle section of the flight leg, consistent with buoyancy wave oscillations (Pierce and Grant, 1998). Like the O3 and theta residuals the u and v residuals (not shown) showed considerable energy at 24 km scales and below. There is little doubt that the oscillations shown by the residual profiles in Fig.10 reflect gravity-wave oscillations, which can lead to efficient mixing across air mass boundaries (Danielsen et al. 1991) and could explain the mixing signatures found in tracer-tracer correlation plots.

6. Conclusions:

In this paper we have used in-situ observations taken from 2 DC8 flights during INTEX-NA to study the characteristics of small-scale structure in the upper troposphere in the vicinity of the subtropical jet. Both flights took place over a similar geographic domain, yet one showed a high degree of small-scale tracer variability on level flight legs, whereas the other did not. When viewed in a reference frame relative to the subtropical jet, the differences became clear. Small-scale tracer structure was particularly pronounced on level flight legs, poleward of the jet core and just beneath the strong tracer gradients defining the tropopause; in contrast such structure was much weaker under an elevated tropopause, equatorward of the jet. Coincident with enhanced small-scale variability, in-situ observations on July 18 showed evidence of interleaving and mixing of stratospheric and polluted tropospheric air in the upper troposphere. On the flight of August 02, the DC8 sampled the low stratosphere on the poleward side of the jet, where an intrusion of polluted air from the troposphere was found.

On the same day, more aged pollution was found in the upper troposphere on the tropical side of the jet. We used trajectory mapping (RDF) of 3-d model (RAQMS) chemical and dynamical fields to demonstrate that filamentary structure, generated via descent and differential advection on the poleward side of the jet, contributed to the sub-grid-scale variability observed in the upper troposphere on July 18. For the case considered here RDF showed skill in refining tracer structure seen in RAQMS analyzed fields. We used Lagrangian averages of a strain-rotation measure, Q, to help distinguish air masses that had experienced shear strain deformation from those subject to more stable rotational conditions. Although deduced filamentary structure was closely aligned with high Q, for the case considered Q by itself provided limited guidance on where high-frequency tracer variability could be expected.

Higher frequency tracer and dynamical structures observed on July 18 were found to be characteristic of gravity wave oscillations. These waves are known to be an efficient vehicle for mixing across tracer gradients. The observation of mixed polluted and stratospheric air mass signatures co-located with gravity wave activity in the upper troposphere on the poleward side of the jet indicates that the gravity waves were responsible for the irreversible mixing of air in the vicinity of the tropopause.

In this study, we do not attempt to quantify the degree of stratospheric exchange with the upper troposphere, nor the extent of mixing across the tropopause during INTEX-NA, but simply to account for some of the mechanisms responsible for observed structure along upper level flight tracks. Thompson et al. (this issue) estimated that 35% of tropospheric O3 was stratospherically influenced in the INTEX domain. Dibb et al. (this issue) estimated from O3-NOy correlations that 34% of air parcels sampled in the upper troposphere during INTEX were stratospherically influenced. Al-Saadi et al. (this issue) showed that much of the stratospheric influence of the troposphere in the INTEX domain originated well upstream in the central Pacific. Fuelberg et al. (this issue) found that 27% of air parcel trajectories from DC8 flight tracks encountered the stratosphere within the previous 10 days. The comparison of observed and

simulated tracer variability and mixing for the cases considered here suggests that the degree of mixing across the troposphere was larger than 3-d models estimate.

References:

Al-Saadi, J. A., R,B. Pierce, T.D. Fairlie, T.K, Schaack, et al., A Lagrangian Characterization of the Sources and Chemical Transformation of Air Influencing the US and Europe during the 2004 ICARTT/INTEX-NA Campaign, this issue.

Al-Saadi, Jassim A., James Szykman, R. Bradley Pierce, Chieko Kittaka, Doreen Neil, D. Allen Chu, Lorraine Remer, Liam Gumley, Elaine Prins, Lewis Weinstock, Clinton MacDonald, Richard Wayland, Fred Dimmick and Jack Fishman. 2005: Improving National Air Quality Forecasts with Satellite Aerosol Observations. *Bulletin of the American Meteorological Society*: Vol. 86, No. 9, pp. 1249–1261.

Appenzeller, C., H. C. Davies, W. A. Norton, Fragmentation of stratospheric intrusions, J. Geophys. Res., 101(D1), 1435-1456, 10.1029/95JD02674, 1996.

Avery, M. A., J. V. Plant and C. H. Hudgins, FASTOZ: An accurate, fast-response in situ ozone measurement system for aircraft campaigns, (2006), submitted, J. Oceanic and Atmos. Tech.

Chameides, W. and D. Davis, Chemistry of the troposphere, Chem. Eng. News, 60 (40): 38-52 1982.

Chan, K. R., Dean-Day, J., Bowen, S. W. and T .P. Bui, “Turbulence measurements by the DC-8 meteorological measurement system”, Geophys. Res. Lett., 25(9), 1355-1358, 1998.

Cho, J. Y. N., R. E. Newell, T. P. Bui, E. V. Browell, M. A. Fenn, M. J. Mahoney, G. L. Gregory, G. W. Sachse, S. A. Vay, T. L. Kucsera, A. M. Thompson, Observations of convective and dynamical instabilities in tropopause folds and their contribution to stratosphere-troposphere exchange, J. Geophys. Res., 104(D17), 21549-21568, 10.1029/1999JD900430, 1999.

Cooper, O. R., C. Forster, D. Parrish, M. Trainer, E. Dunlea, T. Ryerson, G. Hubler, F. Fehsenfeld, D. Nicks, J. Holloway, J. de Gouw, C. Warneke, J. M. Roberts, F. Flocke and J. Moody, “A case study of transpacific warm conveyor belt transport: Influence of merging airstreams on trace gas import to North America”, (2004), J. Geophys. Res., Vol 106, D23S08, doi:10.1029/2003JD003624.

Dibb, J.E., E. Scheur, R. Talbot, M. Avery, Stratospheric Influence on the Composition of the Mid- and Upper-Troposphere over North America sampled by the NASA DC-8 during INTEX A, (2006), this issue.

Danielsen, **E.F.**, R.S. Hipskind, W.L. Starr, et al., Irreversible transport in the stratosphere by internal waves of short vertical wavelength, J. Geophys. Res.,96 (D9): 17433-17452, 1991.

Esler J. G., P. H. Haynes, K. S. Law, H. Barjat, K. Dewey, J. Kent, S. Schmitgen, and N. Brough, Transport and mixing between airmasses in cold frontal regions during Dynamics and Chemistry of Frontal Zones (DCFZ), (2003), J. Geophys. Res., 108 (D4), 4142, doi:10.1029/2001JD001494.

Fairlie, T. D., R. B. Pierce, W. L. Grose, G. Lingenfelser, M. Loewenstein, J. R. Podolske, Lagrangian forecasting during ASHOE/MAESA: Analysis of predictive skill for analyzed and reverse-domain-filled potential vorticity, J. Geophys. Res., 102(D11), 13169-13182, 10.1029/96JD03507, 1997.

Fairlie, T. D., M. H. Proffitt, C. R. Webster, The contribution of mixing in Lagrangian photochemical predictions of polar ozone loss over the Arctic in summer 1997, J. Geophys. Res., 104(D21), 26597-26610, 10.1029/1999JD900111, 1999.

Fehsenfeld, F., ICARTT overview, J. Geophys. Res., ICARTT/INTEX-NA special issue (submitted).

Fishman, J., V. Ramanathan, P.J. Crutzen, and S.C. Liu, Tropospheric ozone and climate, Nature, 282, 818-820, 1979.

Fishman, J., and P. Crutzen, The origin of ozone in the troposphere, Nature, 274, 855-857, 1978.

Forster, P. M. de F., K. P. Shine, Radiative forcing and temperature trends from stratospheric ozone changes, J. Geophys. Res., 102(D9), 10841-10856, 10.1029/96JD03510, 1997.

Fuelberg, H., E.M. Porter, C.M. Kiley, D. Morse, A meteorological overview of the INTEX-A period (this issue)

Haynes, P. H., 1990: High-resolution three-dimensional modelling of stratospheric flows: quasi-two-dimensional turbulence dominated by a single vortex. In: Topological Fluid Mechanics, ed. H. K. Moffatt, Tsinober; Cambridge University Press, 345--354.

Holton, J. R., P. H. Haynes, M. E. McIntyre, A. R. Douglass, R. B. Rood, L. Pfister, Stratosphere-troposphere exchange, Rev. Geophys., 33(4), 403-440, 10.1029/95RG02097, 1995.

Liu, S.C., D. Kley, M. McFarland, J.D. Mahlman, and H. Levy II, On the origin of tropospheric ozone, J. Geophys. Res., 85, 7546-7552, 1980.

Jacob, D. J., and A. Gilliland, Modeling the impact of air pollution on global climate change, Environmental Manager, pp. 24-27, October 2005.

Kim, S., L.G. Huey, R.E. Stickel, D.J. Tanner, J. H. Crawford, J.R. Olson, G. Chen, W. H. Brune, X. Ren, R. Lesher, P. J. Wooldridge, T. H. Bertram, A. Perring, R.C. Cohen, B., B., this issue.

Logan, J.A., M.J. Prather, S.C. Wofsy, and M.B. McElroy, Tropospheric chemistry: a global perspective, J. Geophys. Res., 86, 7210-7254, 1981.

Logan, J.A., Tropospheric ozone – seasonal behavior, trends, and anthropogenic influence, J. Geophys. Res., 90, 10463-10482, 1985.

Norton, W. A., 1994: Breaking Rossby Waves in a Model Stratosphere Diagnosed by a Vortex-Following Coordinate System and a Technique for Advecting Material Contours**.** *J. Atmos. Sci.*: Vol. 51, No. 4, pp. 654–673.

Pierce R.B. and T.D. Fairlie, 1993, Chaotic advection in the stratosphere: Implications for the dispersal of chemically perturbed air from the polar vortex, J. Geophys. Res,. 98(D10), 18589-18,595, 1993.

Pierce, R. Bradley, T. Duncan Fairlie, William L. Grose, Richard Swinbank and Alan O'Neill. 1994: Mixing Processes within the Polar Night Jet. *Journal of the Atmospheric Sciences*: Vol. 51, No. 20, pp. 2957–2972.

Pierce, R. B., and W. B. Grant, Seasonal evolution of Rossby and gravity wave induced laminae in ozonesonde data obtained from Wallops Island, Virginia, Geophys. Res. Lett., 25(11), 1859-1862, 10.1029/98GL01507, 1998.

Pierce R. B., et al., Large-scale chemical evolution of the Arctic vortex during the 1999/2000 winter: HALOE/POAM III Lagrangian photochemical modeling for the SAGE III—Ozone Loss and Validation Experiment (SOLVE) campaign, J. Geophys. Res., 107, 8317, doi:10.1029/2001JD001063, 2002. [printed 108 (D5), 2003]

Pierce R. B., et al., Regional Air Quality Modeling System (RAQMS) predictions of the tropospheric ozone budget over east Asia, J. Geophys. Res., 108 (D21), 8825, doi:10.1029/2002JD003176, 2003.

Pierce, R.B. et al., Chemical data assimilation estimates of continental U.S. ozone and nitrogen budgets during INTEX-NA, this issue

Postel, G.A., and Matthew H. Hitchman. 1999: A Climatology of Rossby Wave Breaking along the Subtropical Tropopause. *Journal of the Atmospheric Sciences*: Vol. 56, No. 3, pp. 359–373.

Shapiro, M.A., 1980: Turbulent Mixing within Tropopause Folds as a Mechanism for the Exchange of Chemical Constituents between the Stratosphere and Troposphere. *Journal of the Atmospheric Sciences*: Vol. 37, No. 5, pp. 994–1004.

Singh et al., Overview of the summer 2004 Intercontinental Chemical Transport Experiment – North America (INTEX-NA), this issue.

Sutton, R. T., Hector Maclean, Richard Swinbank, Alan O'Neill and F. W. Taylor. 1994: High-Resolution Stratospheric Tracer Fields Estimated from Satellite Observations Using Lagrangian Trajectory Calculations. *Journal of the Atmospheric Sciences*: Vol. 51, No. 20, pp. 2995–3005.

Thompson et al., IONS-4: Perspective on summertime UT/LS ozone over Northeastern America, this issue

Thornton, J.A., P.J. Woodbridge, and R.C. Cohen, Atmospheric NO2: In situ laser-induced fluorescence detection at parts per trillion mixing ratios, Anal. Chem., 72(3), 523-539, 10.1021/ac9908905 S0003-2700(99)00890-2, 1999.

Wang, Y., J.A. Logan, and D.J. Jacob, Global simulation of tropospheric O3-Nox-hydrocarbon chemistry. 2. Model evaluation and global ozone budget. J. Geophys. Res., 103, D9, 10,727-10,755,1998.

Waugh, D.W., and R. Alan Plumb. 1994: Contour Advection with Surgery: A Technique for Investigating Finescale Structure in Tracer Transport. *Journal of the Atmospheric Sciences*: Vol. 51, No. 4, pp. 530–540.

Zapotocny, T.H., Donald R. Johnson, Fred M. Reames, R. Bradley Pierce and Bart J. Wolf. 1991: Numerical Investigations with a Hybrid Isentropic Sigma Model. Part II: The Inclusion of Moist Processes. *Journal of the Atmospheric Sciences*: Vol. 48, No. 18, pp. 2025–2043.

Zapotocny, T.H., D.R. Johnson, F.M. Reames, Development and initial test of the University of Wisconsin Global Isentropic-Sigma Model, Mon. Wea. Rev., 122, 2160-2178, 1994

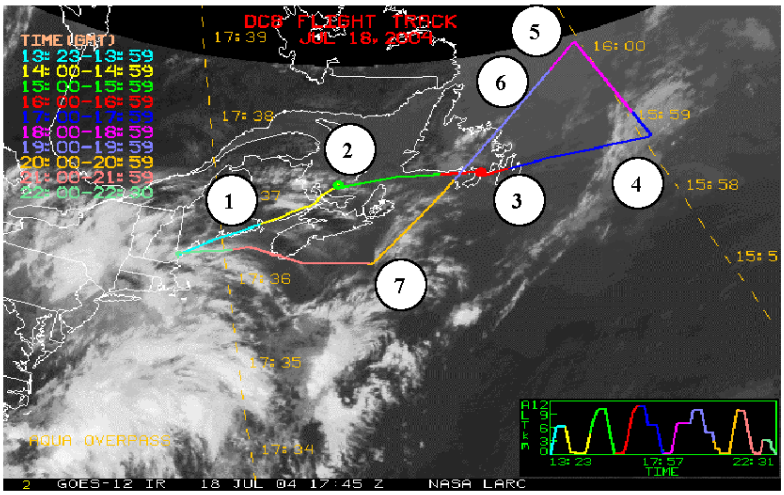

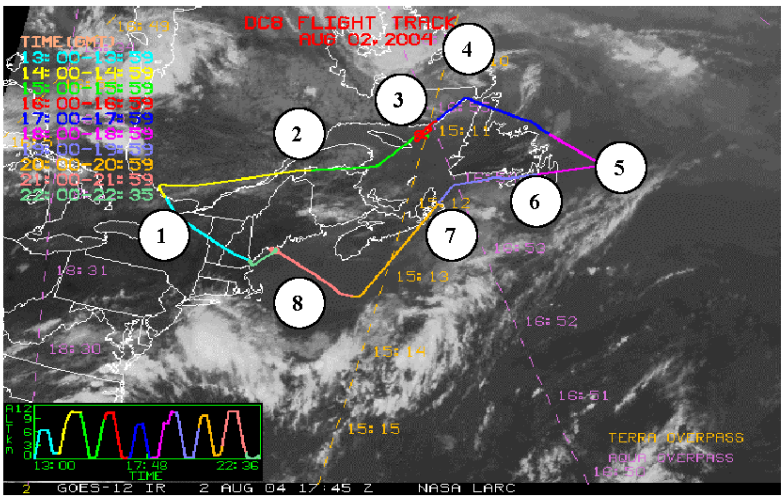

1
2 Figure 1: NOAA GOES 12 IR water vapor image for 1745Z on (a) July 18 and (b)
3 August 2 with overlaid DC9 flight tracks. Altitude profiles for the flights are inset.
4 Level flight legs are numbered 1-7 and 1-8 respectively for each of the two
5 flights. (Courtesy D. Westberg, SAIC)
6

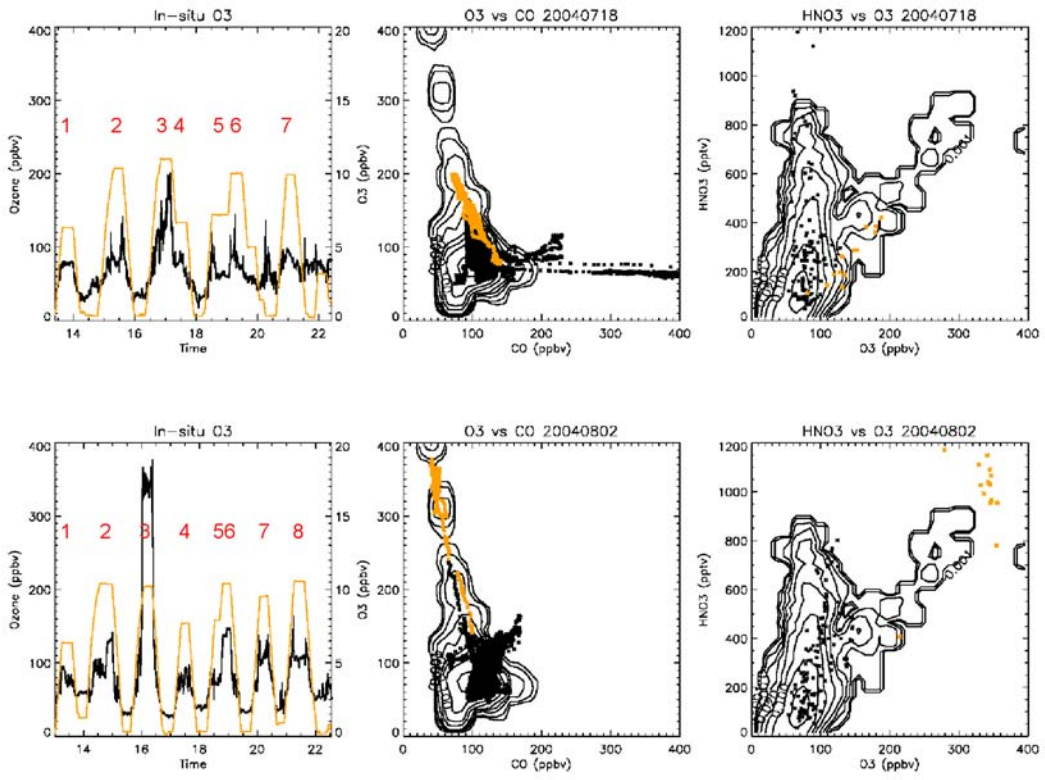

Figure 2: Time series of in situ O3 for 18 July and 02 August (black) with DC8 altitude profiles (km-ordinate on right) (orange). Scatter plots of in situ O3 vs. CO and HNO3 vs. O3 for points above 500 mbar for the same days, together with 2-d pdfs of all such points for remaining flights between 06 July and 10 August (contoured). Data points for FLs 3 on each day are highlighted (orange).

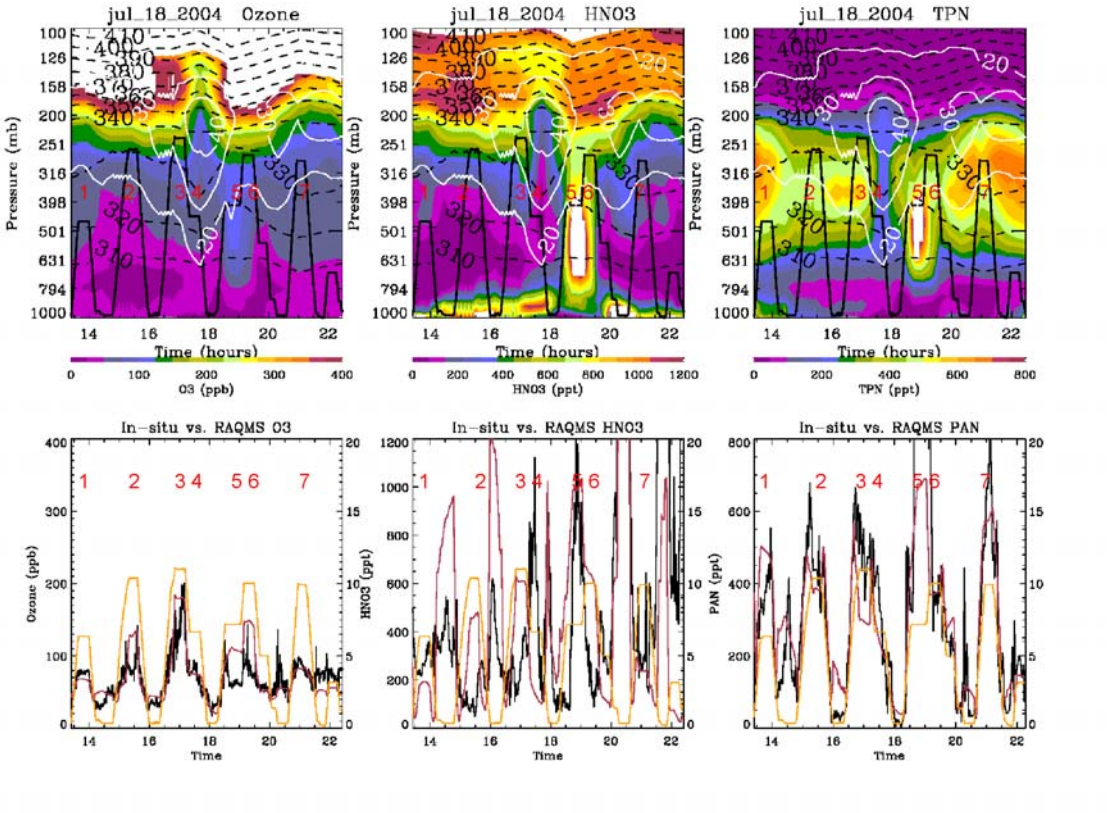

Figure 3: (a) Curtains of RAQMS ozone, HNO3, and TPN along the DC8 flight track, with flight profiles superimposed, for July 18 (upper panels). Corresponding time series of observed (black) and RAQMS (red) flight track data are also shown (lower panels). Flight track altitude is shown in orange.

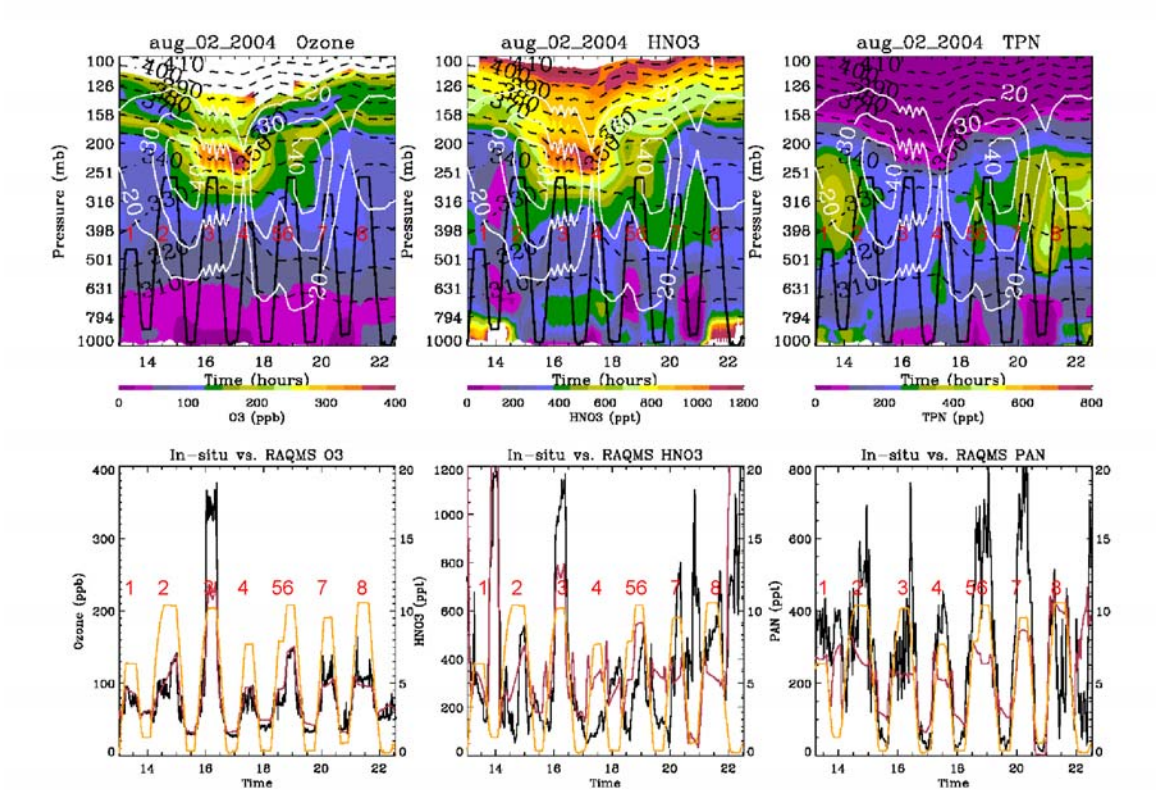

Figure 3: (b) As for Fig.3a, but for 02 August.

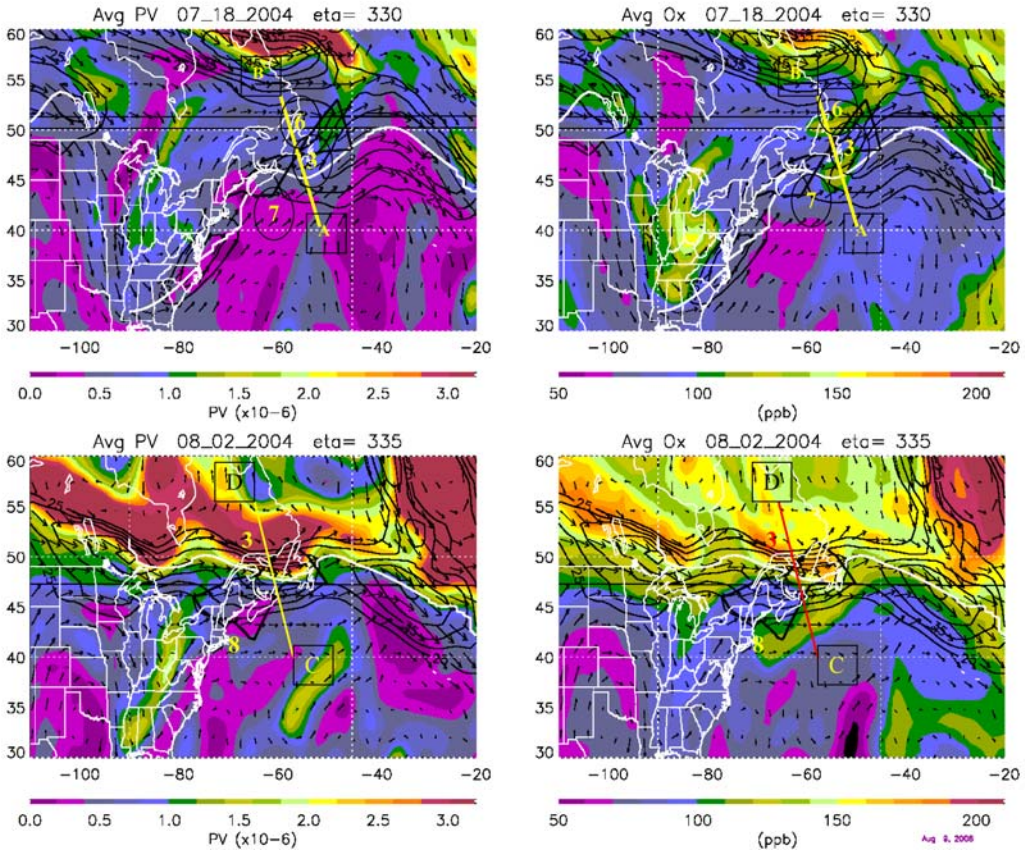

Figure 4: Maps of PV and O3 from RAQMS for 18Z on July 18 for the 330K eta surface (top panels), and on 02 August for the 335K eta surface (lower panels). Isotachs (black contours), wind arrows, the DC8 flight track (black), and selected flight legs are also shown. Lines A-B and C-D mark cross-sections shown in Figs. 5(a) and (b).

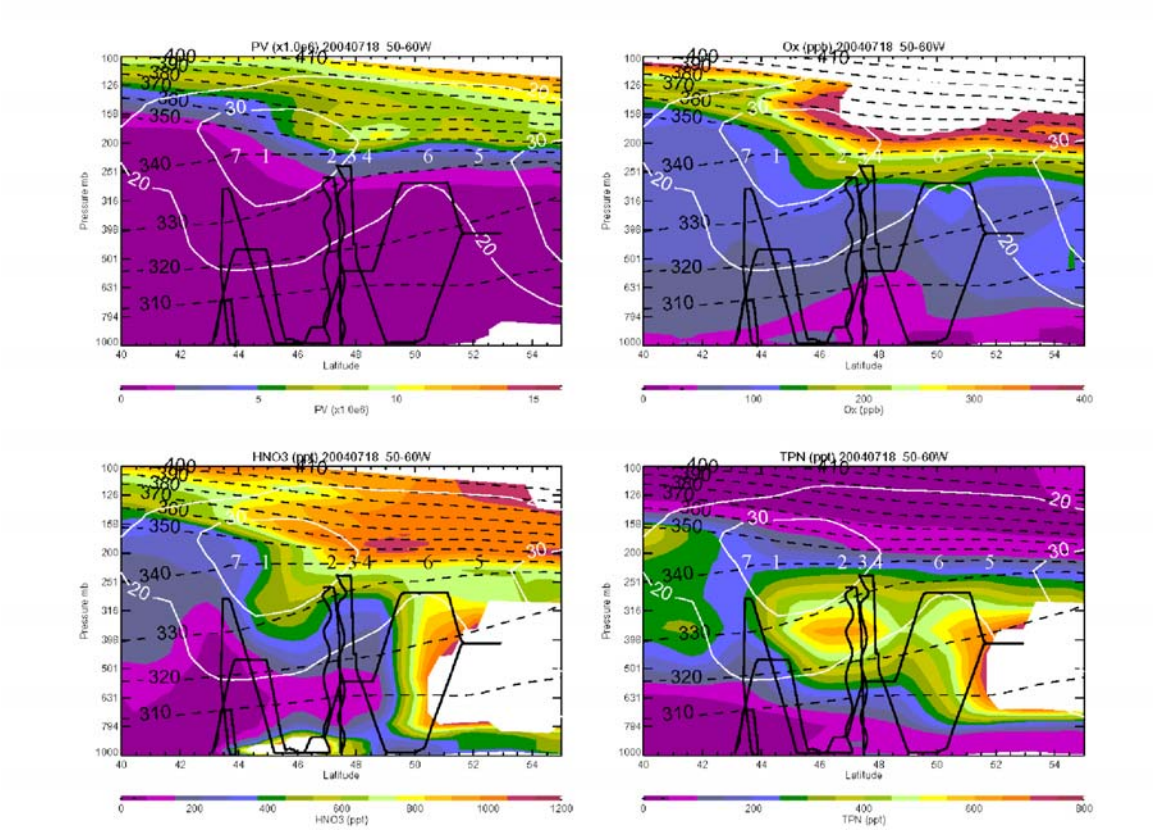

Figure 5: (a) Cross-sections of RAQMS PV, O3, HNO3, and TPN at 18Z on July 18 taken along the line marked A-B in Figure 4. Isotachs (white) and isentropes (black dashed) are also shown. The flight altitude profile is projected on to the section (black) Upper level FLs are marked. The A-B section crosses the flight track near FL 3.

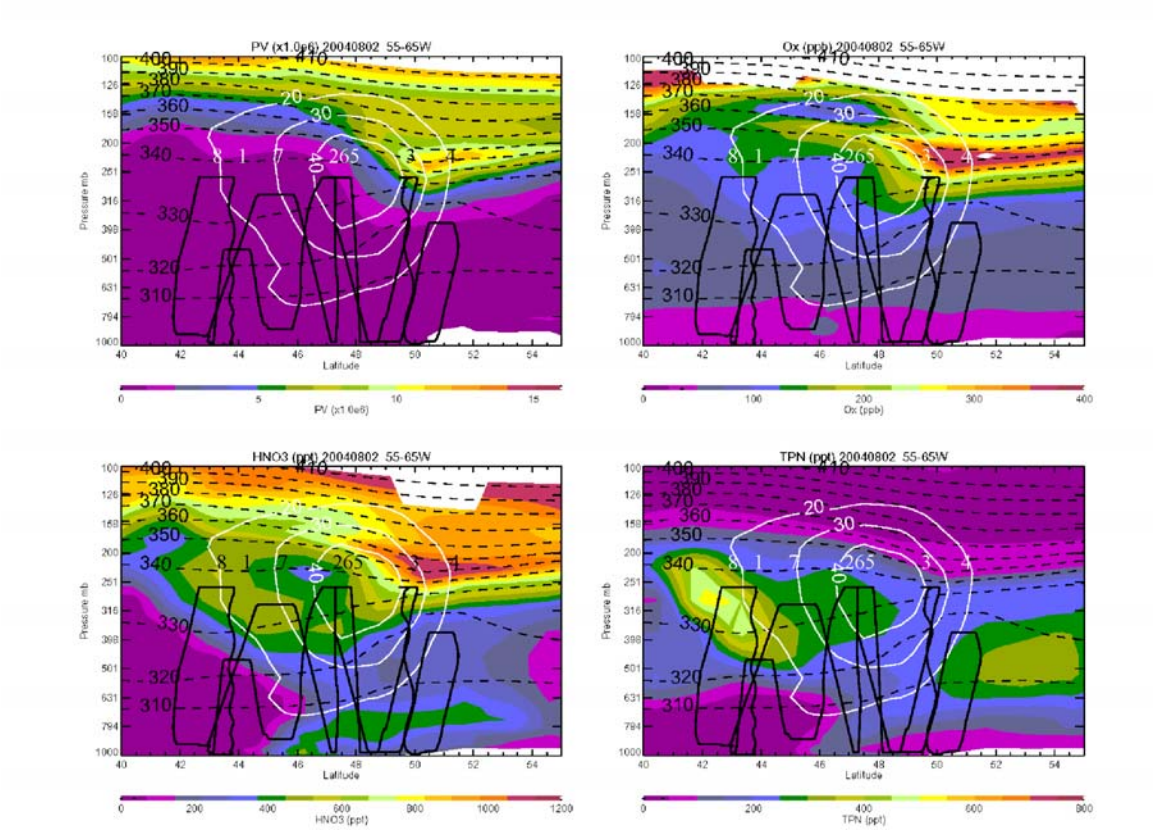

Figure 5: (b) As for Fig.5(a), but cross-sections are along line C-D in Fig.4 for 02 August.

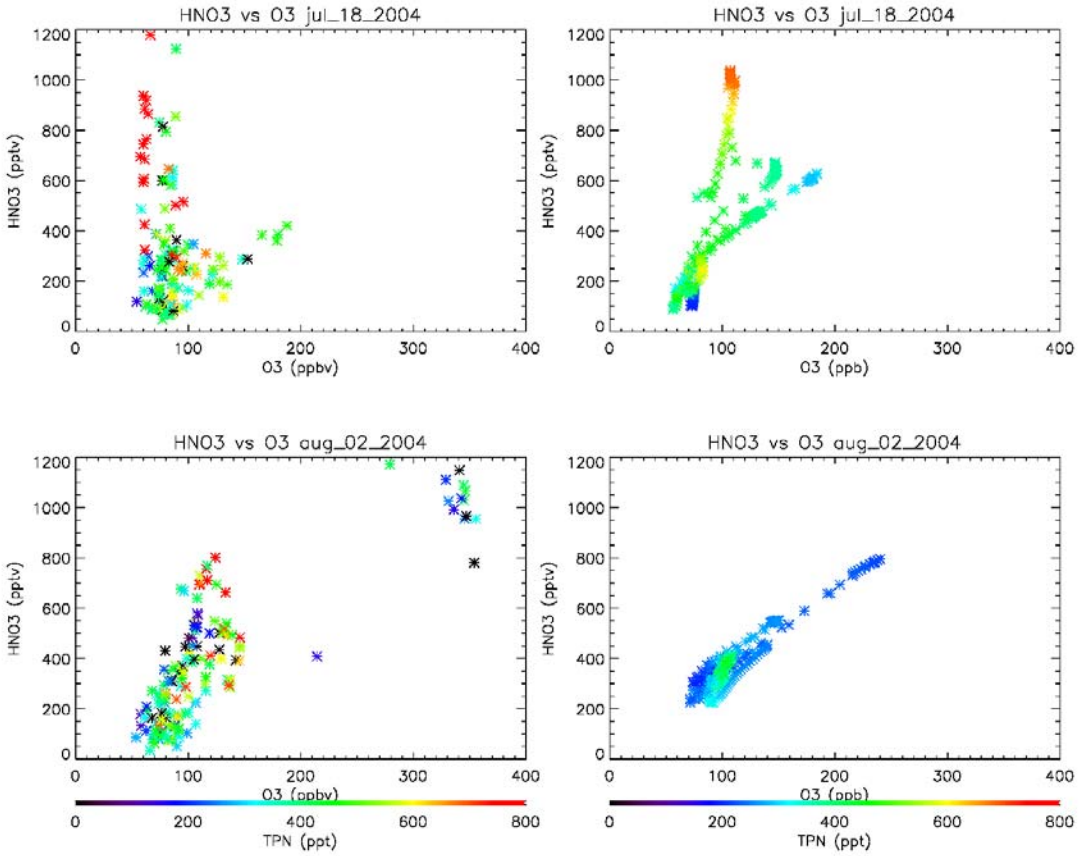

Figure 6: Scatter plots of in situ (left) and simulated (right) HNO3 vs. O3 for July 18 (top) and August 02 (bottom). All points are located above 500 mb. The points are colored by observed and simulated TPN mixing ratio, respectively.

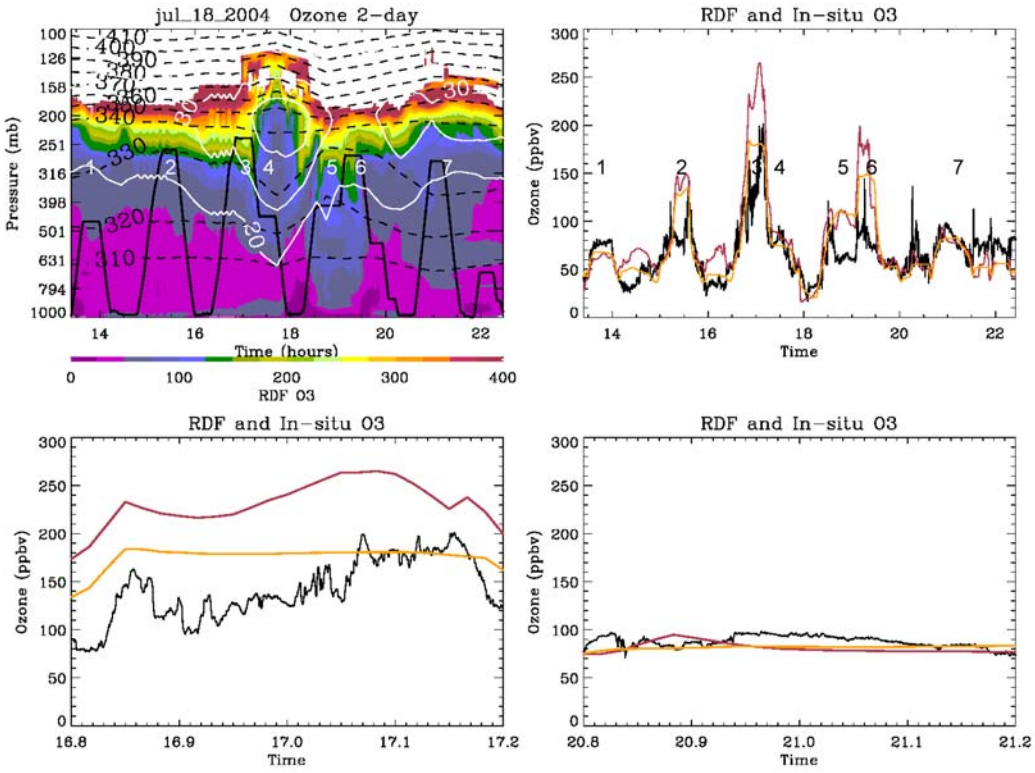

Figure 7: 2-day RDF ozone along the flight curtain from RAQMS for July 18. Potential temperature contours (black dashed) and isotachs (white) are also shown, together with the flight altitude. Top right panel shows time series of 1-sec in situ ozone (black) together with RAQMS analyzed (yellow) and 2-day RDF (red) ozone. Lower panels show time series as above but focused on FLs 3 (left) and 7 (right).

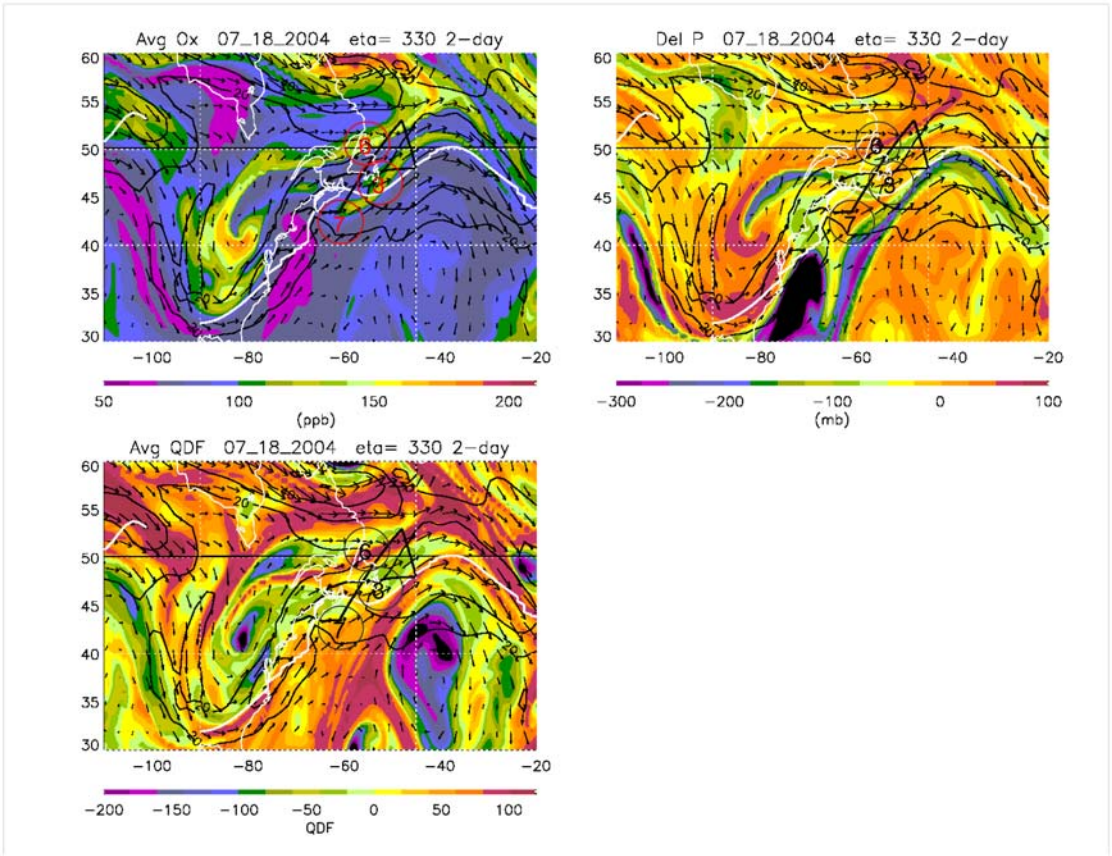

Figure 8: 2-day RDF maps of ozone, and Q at 330K with 2-day map of Lagrangian Δp for 18Z on 18 July. Isotachs (black contours), wind arrows, and the flight track on 18 July (black) with selected FLs are also shown. White lines mark the axis of strongest winds on the 330K surface in each map.

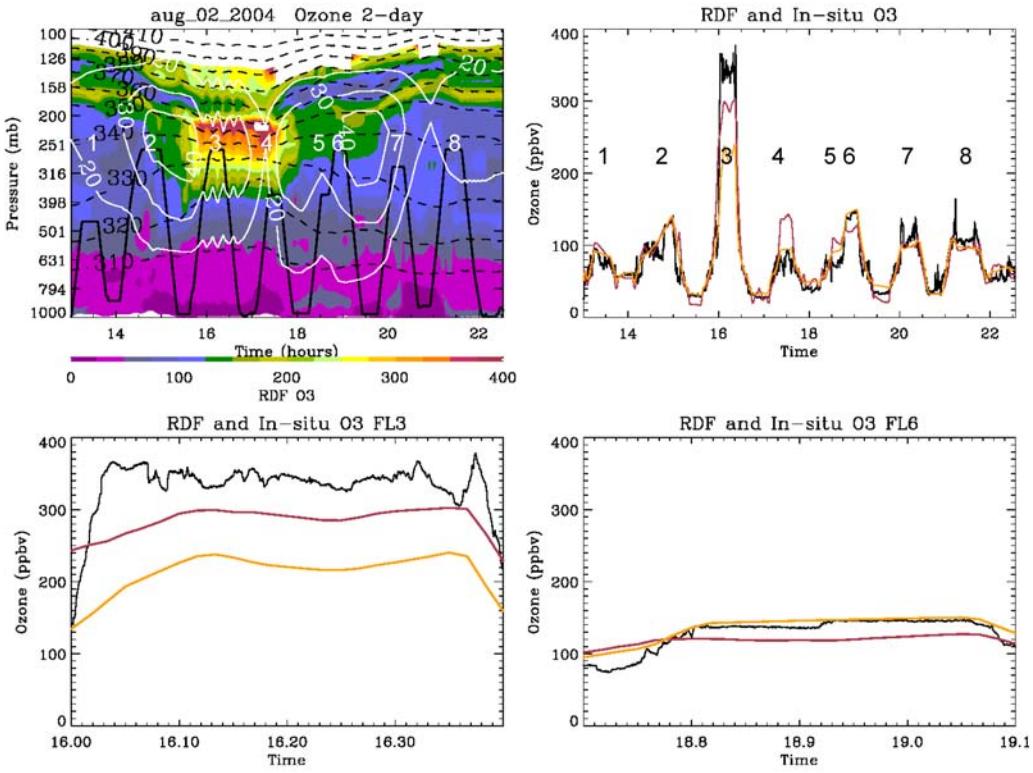

Figure 9: 2-day RDF ozone along the flight curtain from RAQMS for August 02. Potential temperature contours (black dashed) and isotachs (white) are also shown, together with the flight altitude. Top right panel shows time series of 1-sec in situ ozone (black) together with RAQMS analyzed (yellow) and 2-day RDF (red) ozone. Lower panels show time series as above but focused on FLs 3 (left) and 6 (right).

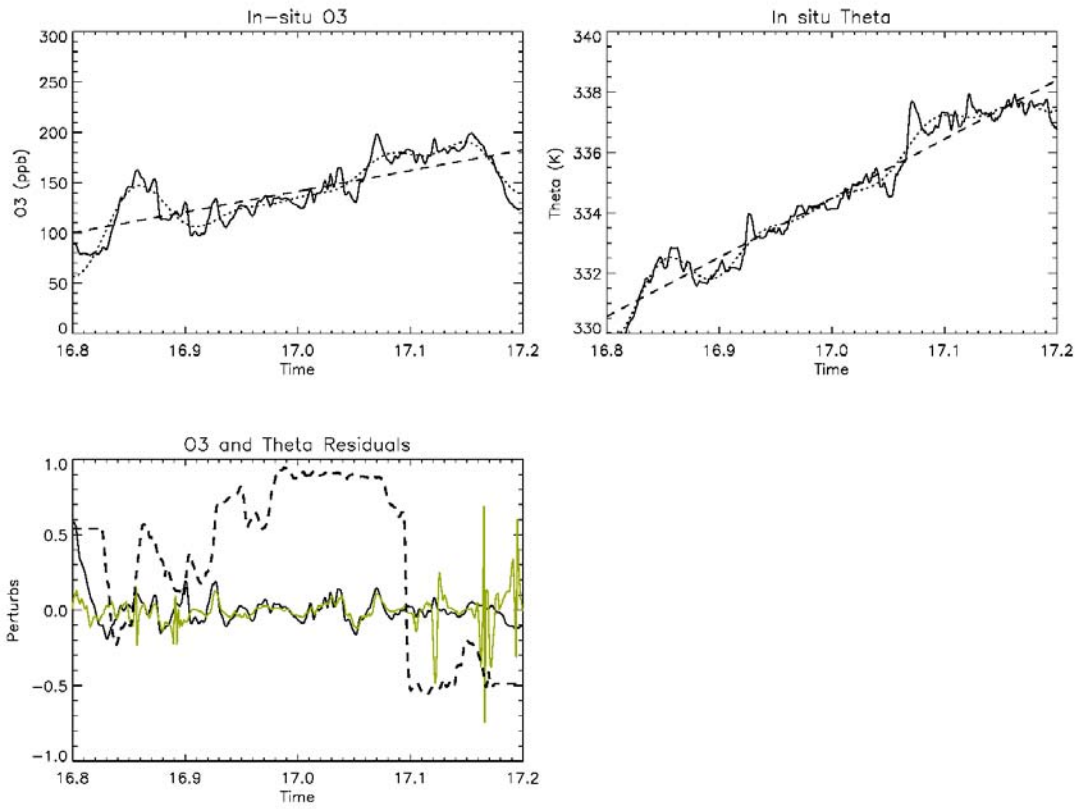

Figure 10: Analysis of in situ O3, and theta, for FL3 on 18 July: Top panels show time series of 10-sec. O3 and theta, together with linear trends (dashed), and medium-pass-filtered data (dotted). Lower panel shows normalized residuals of O3 and theta data with medium-pass-filtered data removed. The theta residuals are multiplied by a scaling factor (see text for details). Also shown is the correlation between the residuals (dashed).